

An Adaptive Window for Stare Processing of Delay Doppler Maps

Benjamin J. Southwell and Andrew G. Dempster

ABSTRACT

GNSS-R is the use of reflected Global Navigation Satellite System (GNSS) signals for remote sensing. Stare processing is a technique which focuses on a fixed point on the ocean surface as it traverses through contiguous Delay Doppler Maps (DDM). As the stare point moves through the DDM and spatial domain, the footprint of its ambiguity function varies. This is analyzed and shown to be suboptimal. In this paper a variable length window in the DDM which provides an improved spatial footprint is introduced. The window is varied in length along the delay dimension as the spatial footprint becomes delay limited when the stare point moves away from the specular point. The cross-track resolution is found to be sensitive to the variable delay window whilst a Doppler resolution of 500Hz causes the along-track resolution to be insensitive to the variable delay.

KEYWORDS: GNSS-R, Reflectometry, Stare Processing

1 INTRODUCTION

Global Navigation Satellite Systems (GNSS) signals reflected off the Earth were first proposed for remote sensing applications in 1993 by Martin-Neira [Martin-Neira, 1993]. This is known as GNSS Reflectometry (GNSS-R). Multiple applications of GNSS-R have been proposed and experimental results obtained for altimetry [Martin-Neira, 1993], ocean surface wind vector determination [Gleason, 2006], soil moisture content measurement from both ground based [Rodriguez-Alvarez et al., 2009, Arroyo et al., 2014] and spaceborne receivers [Camps et al., 2016] in addition to sea ice detection [Schiavulli et al., 2017] amongst others.

Ocean scatterometry with spaceborne receivers for the retrieval of mean square slopes (MSS) of the sea surface and surface wind speeds is an active area of research. Currently the TechDemoSat-1 (TDS-1) [Foti et al., 2015] and CYGNSS [Ruf et al., 2012] satellite provide MSS and wind speed

estimation as well as a platform for research, leveraging experience gained from the UK-DMC mission [Gleason et al., 2005, Clarizia et al., 2009].

The area on the ocean surface which reflects a signal towards the receiver is known as the glistening zone. The glistening zone surrounds the specular point which is the point through which the reflected path length is shortest and the incident and reflected vectors satisfy Snell's law of reflection. The scattering frame is defined with its origin at the specular point and xy plane tangent to the surface of the Earth with the x axis positive in the direction of the receiver and z axis normal to the surface.

The rougher the ocean surface, the larger the glistening zone, as it's more likely a surface facet away from the specular point oriented in a way that will accommodate a reflection towards the receiver. The delay and Doppler of surface coordinates in the glistening zone varies causing the received power to be spread in both delay and Doppler. Most of the points on the surface ambiguously map to coordinates in the delay-Doppler domain complicating efforts for inversion. However, there is a line on the surface where unique coordinates exist and a one-to-one mapping occurs; this is known as the ambiguity free line (AFL).

A receiver correlates the reflected signal with a range of local replicas with varying delay and Doppler values in a fashion similar to the acquisition process in a navigation receiver. This produces a Delay Doppler Map (DDM). The received power is a function of the roughness of the ocean surface in addition to factors that parameterize the scattering scenario [Zavorotny and Voronovich, 2000].

$$\langle |P_R(\tau, f_d)|^2 \rangle \propto \int \int_A \sigma^0 \frac{G_R}{R_R^2 R_T^2} \chi^2(\tau, f_d) dA \quad (1)$$

where

- P_R is the received signal power.
- χ is the Woodward Ambiguity Function (WAF)
- τ and f_d are delay and Doppler co-ordinates respectively
- G_R is the gain of the receivers antenna
- R_T and R_R are the distances between the reflecting facet and the transmitter and receiver respectively.
- σ^0 is the extended radar cross section

The integral is performed over the glistening zone A . The ambiguity function for L1 GPS C/A code is

$$\chi^2(\tau, f) \simeq \Lambda^2(\Delta\tau) |S(\Delta f)|^2 \quad (2)$$

where Λ is the autocorrelation function of C/A code and S is the sinc function.

The extended radar cross section σ^0 is the mechanism for representing the roughness of the ocean

surface in the bi-static radar equation [Zavorotny and Voronovich, 2000].

$$\sigma^0 = \frac{\pi |\mathfrak{R}|^2 q^4}{q_z^4} P\left(\frac{q_{\perp}}{q_z}\right) \quad (3)$$

where \mathfrak{R} is the Fresnel reflection coefficient, q is the bistatic vector, q_{\perp} is the horizontal component of q and q_z the vertical, and P is a Gaussian PDF parameterized by the MSS of the sea surface. The bistatic vector is defined as the bisector of the anti-incident and reflected vector.

2 STARE PROCESSING

Stare processing is a technique proposed by [Jales, 2012] and involves taking multiple looks at a fixed point on the Earth's surface over a series of contiguous DDMs. The stare point is chosen so that it lies on or very close to the AFL in all of the DDMs so a one to one inversion can be achieved. Stare processing has been applied to TDS-1 data for MSS retrieval by [Tye et al., 2016] with promising results. Stare profiles extracted from TDS-1 data can last up to 20 seconds long. TDS-1 produces DDMs at 1Hz so stare profiles can have up to 20 data points. Due to the motion of the specular point, the stare point moves through the delay-Doppler domain during the stare profile. This movement also provides multiple looks of the same patch of ocean surface at various incidence angles.

Conversely, the processing of DDMs as part of the CYGNSS mission average the signal minus noise power (SMN) of a fixed window centred around the specular zone over multiple DDMs [Clarizia and Ruf, 2016, Ruf et al., 2016]. This results in the spatial footprint being blurred in the downtrack direction. The maximum number of DDMs to be used in the averaging process is 5 at nadir scattering geometries and drops to 1 at when the incidence angle is approximately 50° [Ruf et al., 2016].

In this paper, data collected by TDS-1, in particular the RD35, track 49 data is investigated and used for illustrative purposes. A 20 second time series is used where the stare point was chosen so that it would coincide with the specular point at the centre of this interval. Over the duration of the stare the incidence angle varies from 11.3° to 12.4° . In this particular profile, the receiver velocity is approximately 40° counterclockwise from the x axis of the scattering frame. In Fig. 1 the movement of the stare point through multiple scattering frames is depicted. The stare point enters the glistening zone at a high delay and a high Doppler and leaves at a high delay and low Doppler over the course of the stare. When $t = 0$, specular coincidence occurs as the stare point is equal to the specular point.

The stare point is chosen to be coincident with the specular point midway through the stare profile so that it does not diverge too far from the AFL. If the stare point is located on the AFL then it is at the lowest delay value possible for any given Doppler. Thus the stare point will traverse the leading edge of the DDM over the course of the stare profile. This can be seen in Fig. 2 where a single cell selected by the stare point is highlighted. The DDMs produced onboard TDS-1 have a delay resolution of approximately 0.25 chips and a Doppler resolution of 500Hz.

At each point in the stare profile, the measured SMN value is recorded, generating the stare profile.

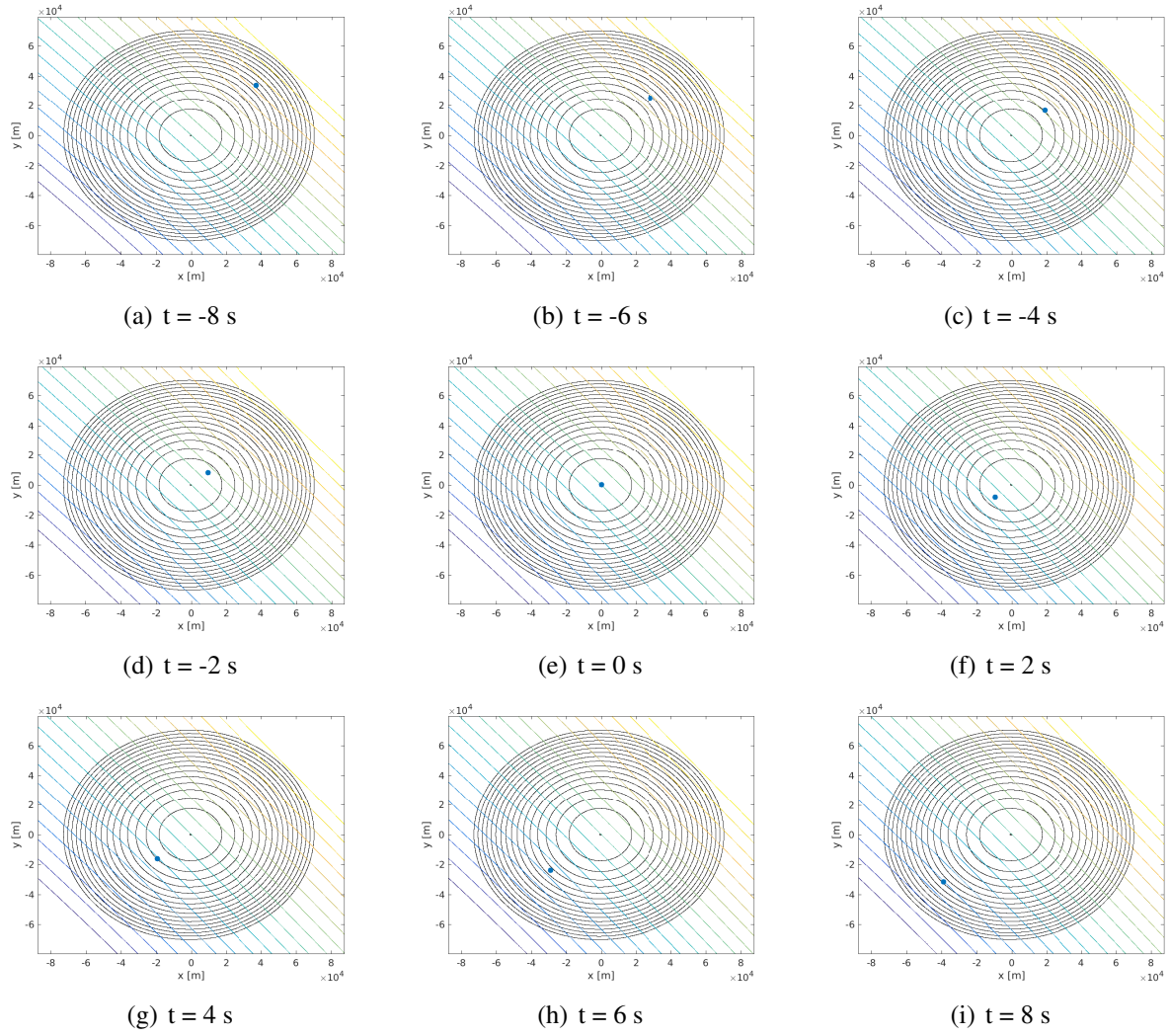
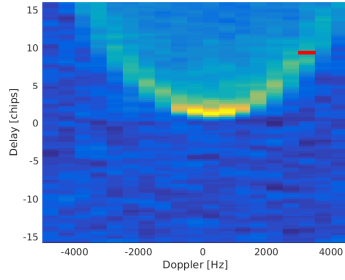
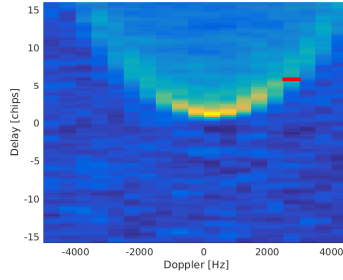


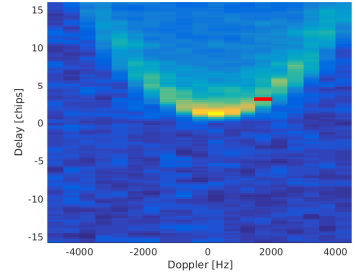
Figure 1: The movement of the stare point in scattering frames during a stare profile.



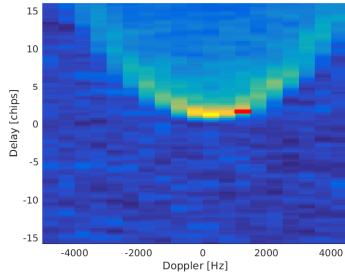
(a) $t = -8$ s



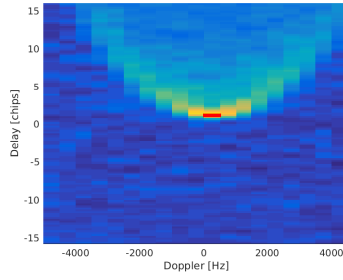
(b) $t = -6$ s



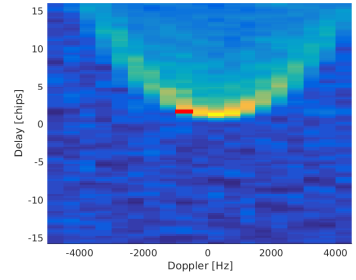
(c) $t = -4$ s



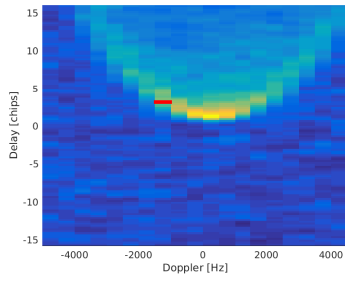
(d) $t = -2$ s



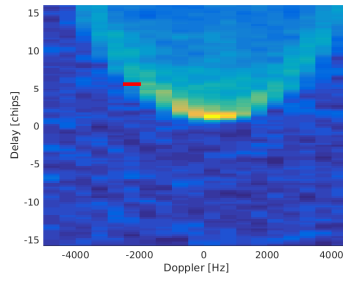
(e) $t = 0$ s



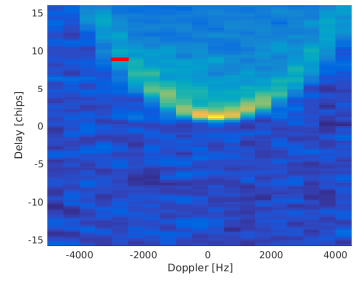
(f) $t = 2$ s



(g) $t = 4$ s



(h) $t = 6$ s



(i) $t = 8$ s

Figure 2: The movement of the stare point in the DDM during a stare profile.

The SMN is proportional to the scattering co-efficient σ^0 and the remainder of the terms in (1) are represented by Γ .

$$SMN \propto \sigma^0(\mathbf{p}) \Gamma(\mathbf{p}) \quad (4)$$

As the stare point moves through the delay-Doppler domain, its WAF response in the spatial domain changes. The WAF footprint of the stare point defines the area of the surface which contributes to the observed signal power at the stare point. The WAF footprint is found by integrating (2) over the xy plane of the scattering frame.

In Fig. 3 the WAF footprint is shown as the stare point moves through the scattering frames. The bounding boxes of the WAF footprint are shown in red. They are defined by considering only the area which has a WAF response of at least -10dB relative to the peak value. It can be seen that, apart from when specular coincidence occurs, the WAF footprints do not correlate well with the bounding boxes. The WAF footprint also grows in the cross-track direction as the stare point moves away from the specular point.

The box is indicative of the actual spatial resolution achievable when producing gridded data products. The box footprint does not vary much in the along-track direction which is ideal as the receiver motion results in different stare points all being located along-track from one another at intervals that can be assumed to be regular in the neighborhood of a small number of stare points. However, the WAF footprints thin out along-track at larger delay values resulting in the WAF footprint area peaking at specular coincidence. It can be seen in Fig. 3 that the WAF footprint is always less than the box footprint.

3 ADAPTIVE WINDOW STARE PROCESSING

The WAF footprint of the stare point defines the area which contributes to the measured signal. The traditional stare processing technique results in the WAF footprint decreasing in size whilst the box footprint increases as the stare point moves away from specular coincidence. Ideally, the WAF footprint would remain constant over the stare profile whilst completely correlating with the box footprint. Fig. 3 indicates that over the course of the stare, some WAF footprints could be extended with minimal impact on the box footprint. This is the motivation for a variable window in the delay-Doppler domain.

The delay increases exponentially as the stare point moves further away from the specular point and the regularly spaced iso-range annuli become more compact in the spatial domain. Additionally, the 500Hz Doppler resolution imposed by the coherent integration time results in the WAF footprint quickly becoming delay limited. Thus, the window in the delay-Doppler domain is proposed to have a variable length in the delay dimension. Looking at Fig. 3 it can be seen that extending the WAF footprint in delay would result in better correlation with the box footprint as the stare point moves away from the specular point. The variable window length chosen is shown in Fig. 4 which is applied to the DDMs of the same stare profile sequence in Fig. 5. This was chosen experimentally.

The WAF footprint resulting from the new variable length window is depicted in Fig. 6 where better

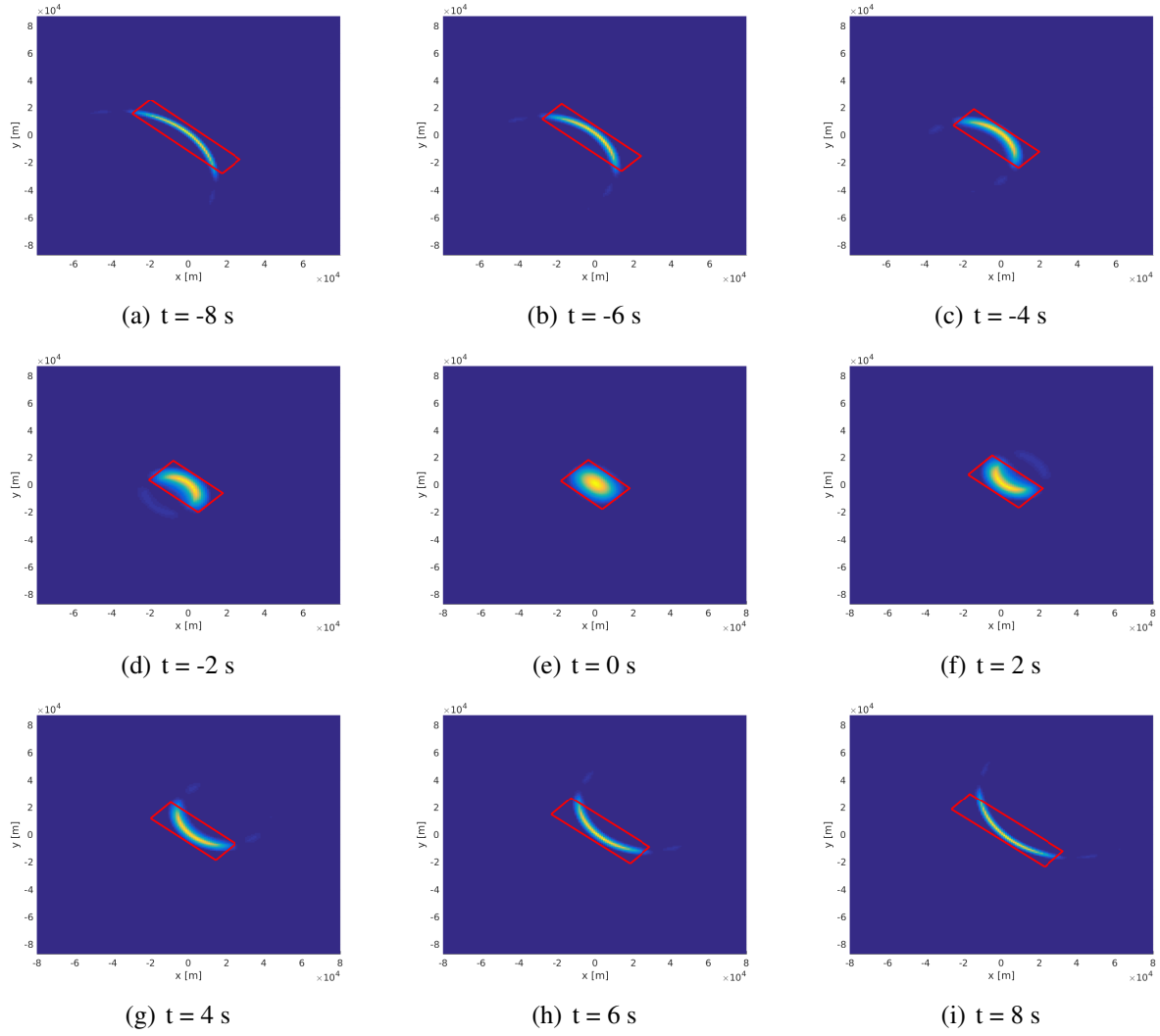


Figure 3: The footprint of the WAF function.

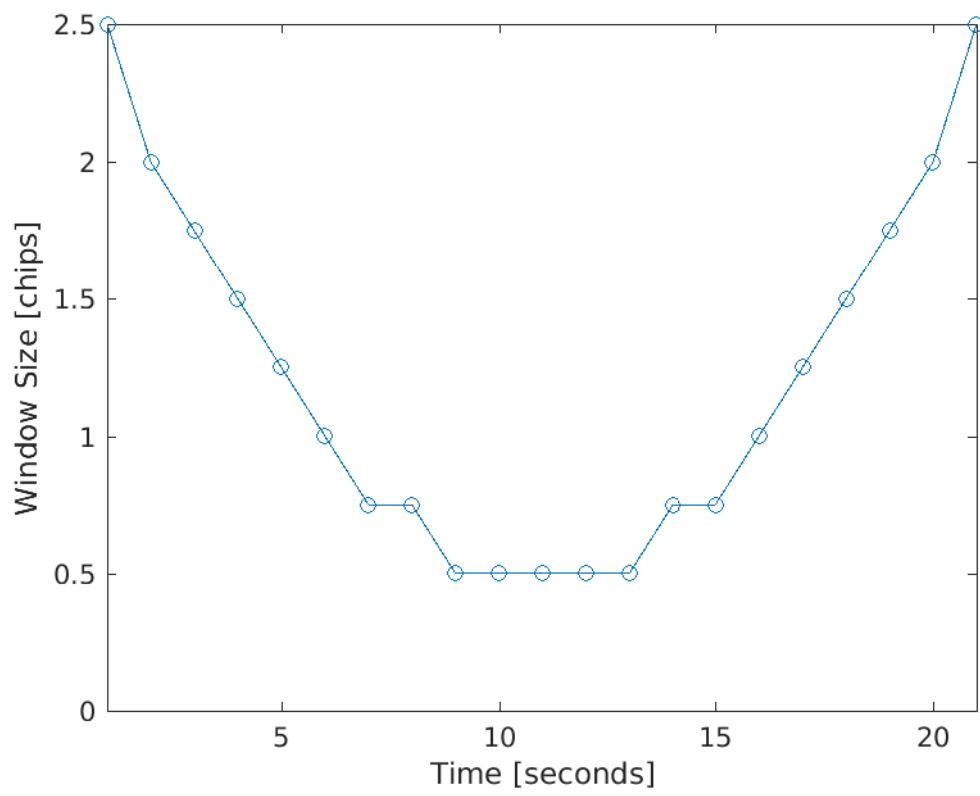
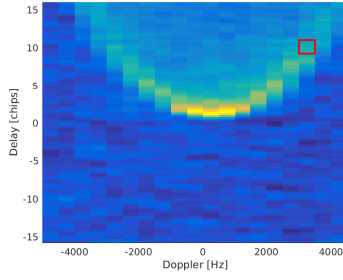
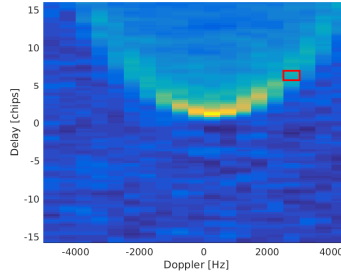


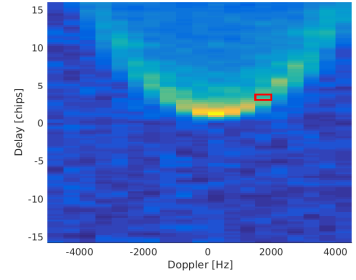
Figure 4: The variable window length over the time of the stare.



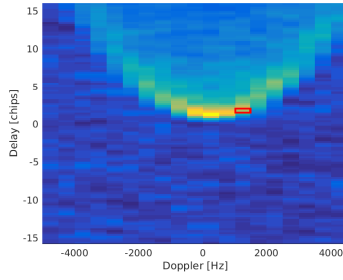
(a) $t = -8$ s



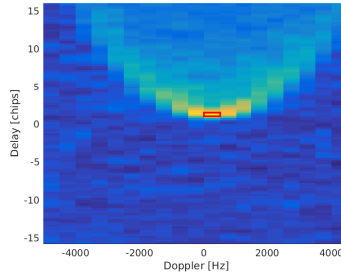
(b) $t = -6$ s



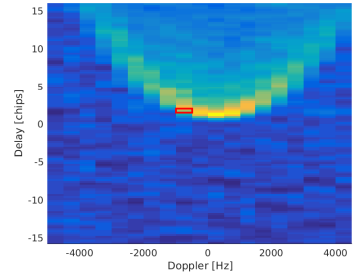
(c) $t = -4$ s



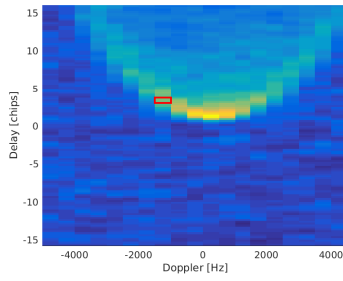
(d) $t = -2$ s



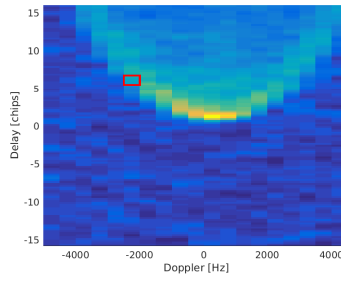
(e) $t = 0$ s



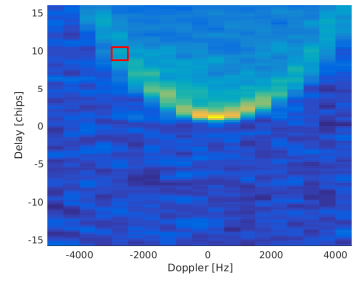
(f) $t = 2$ s



(g) $t = 4$ s



(h) $t = 6$ s



(i) $t = 8$ s

Figure 5: The movement of the variable window in the DDM during a stare profile.

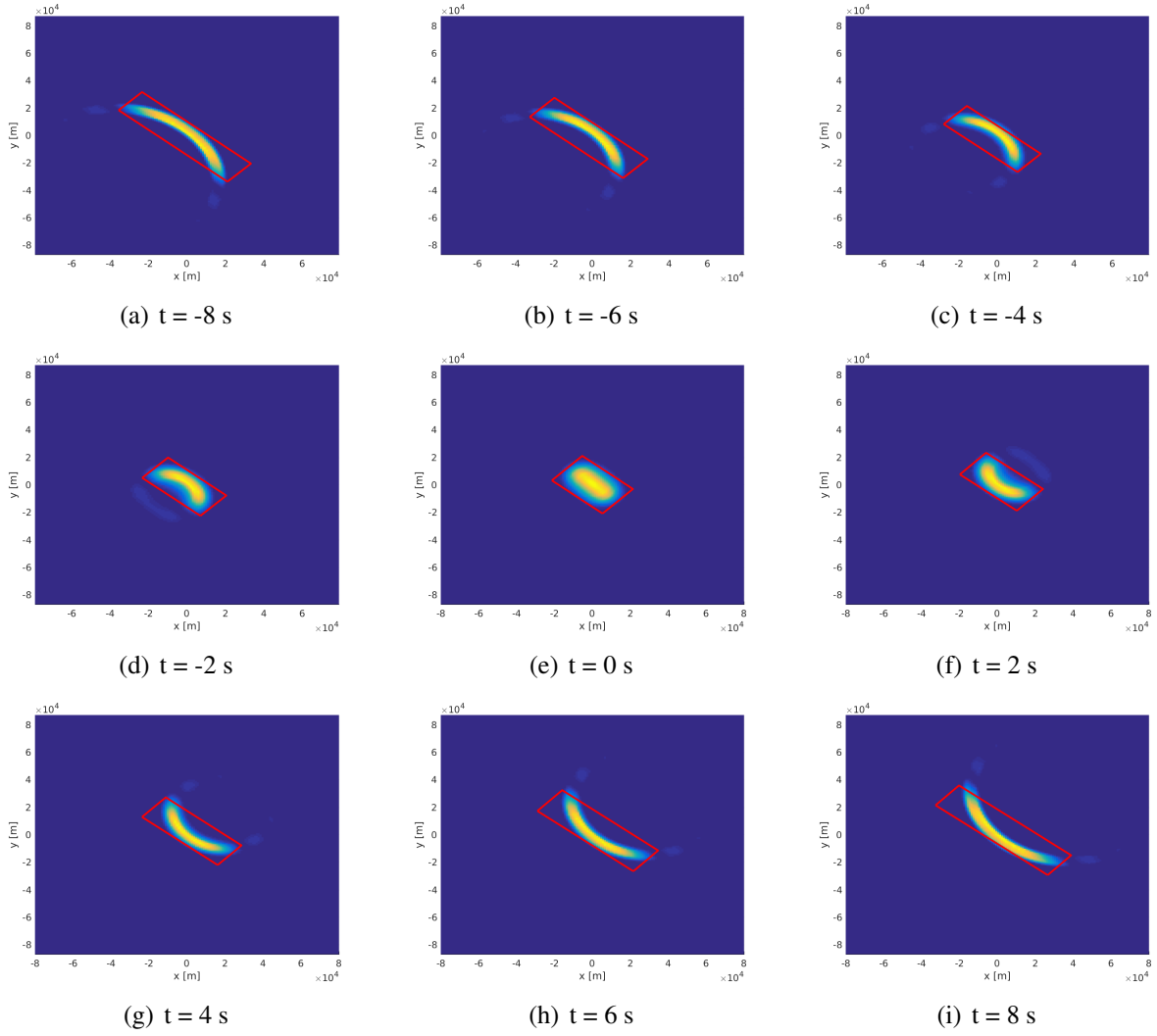


Figure 6: The footprint of the WAF function with a variable delay window length.

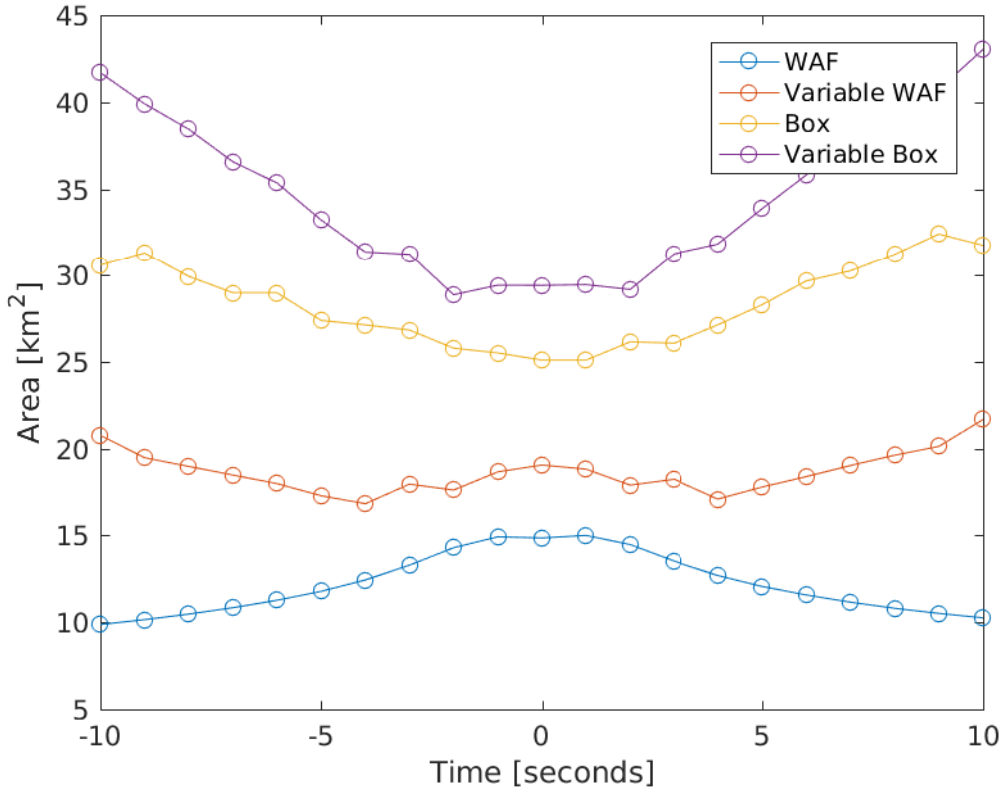


Figure 7: The area of the WAF and box footprint for both regular stare processing and the variable window stare processing method.

correlation between the footprints can be seen. Fig. 7 shows the area of the WAF and box footprints for both the variable window and traditional fixed window stare points throughout the stare profile. The WAF footprint area of the regular stare profile peaks at specular coincidence. While it is nearly constant when the variable window is used resulting in a mean size of 24.43km^2 and a standard deviation of 1.53km^2 . When using the variable window, the box footprint is significantly larger when the stare point moves away from the specular point. However, Fig. 8 shows that the ratio of the WAF footprint area to the box footprint area is improved with the variable window.

Fig. 9 shows the width and length of the box footprint for both stare processing methods. The increased box footprint with the variable window is a result of a combined increase in both the width and length of the box. The box width is in the cross-track direction and the difference between the two widths grows as the stare point moves away from specular coincidence. The receiver motion dominates the iso-Doppler lines resulting in the cross-track resolution being delay limited. Thus, the variable window results in the footprint increasing in the cross-track direction as the stare point moves away from specular coincidence.

The box length is the along-track resolution and remains relatively constant over the course of the stare. The orientation of the iso-Doppler lines result in the along-track resolution being Doppler limited and the variable delay having an insignificant impact. Due to the motion of the specular point in the along-track direction, a ground track of a particular GNSS satellite will allow multiple

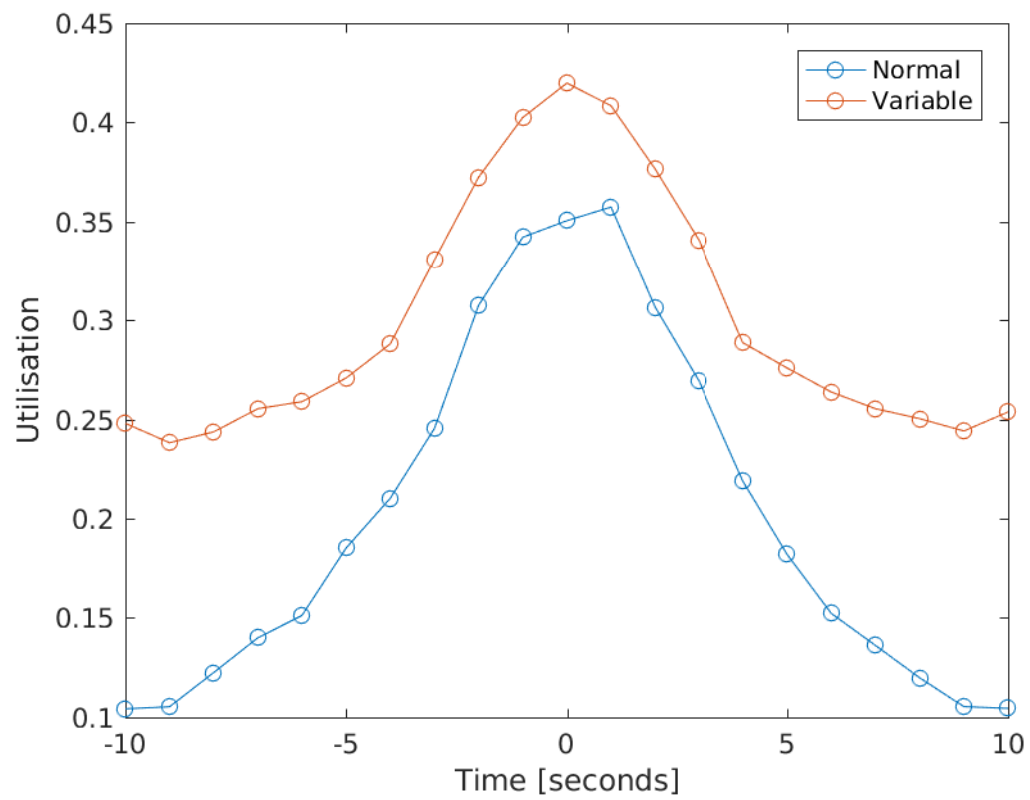


Figure 8: The ratio of the WAF footprint area to the box footprint area. Ideally this should be unity.

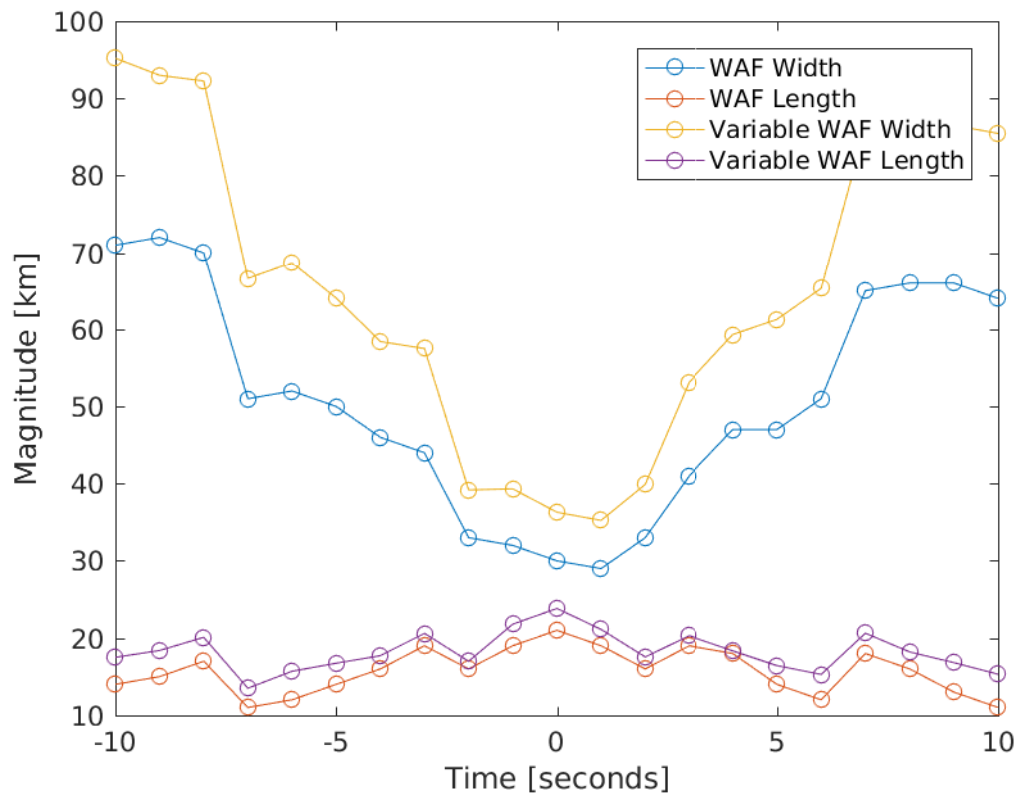


Figure 9: The width and length of the box footprints of the regular WAF and the WAF produced with a variable window. The width and length correspond to cross-track and along-track resolution respectively.

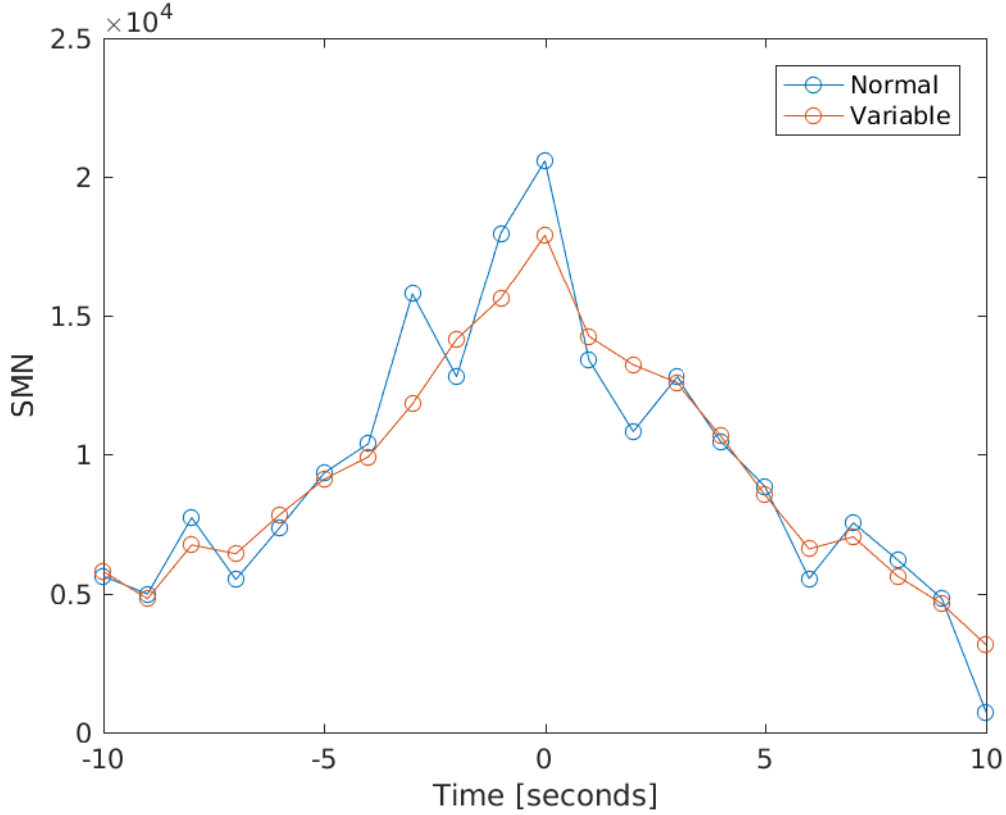


Figure 10: The signal minus noise values of the single chip stare window and the variable length window throughout a stare profile

stare points to be selected in the along-track direction so that coverage is continuous. While the separation of stare points in the cross-track direction is dependent on the relative scattering geometry of multiple GNSS ground tracks. Stare points will be separated by much larger distances in the cross-track direction than the along-track direction. If we assume the sea state to be stationary over scales up to 100 km then the configuration of the footprint produced with the variable window is acceptable for stare processing

In addition to providing an improved spatial footprint, the variable length window will also smooth the observables extracted from the DDM. Fig. 10 shows that the variable window reduces the noise in the SMN stare profile extracted to generate the stare profile.

4 CONCLUSION

Stare processing has previously been applied successfully to data collected by TDS-1. In this paper, a fixed window in the DDM has been shown to produce a WAF footprint which is suboptimal due to it becoming increasingly delay limited as the stare point moves away from specular coincidence. A variable window in the delay-Doppler domain was proposed to optimize the footprint throughout the stare profile.

The variable window stare processing method has shown to keep the WAF footprint area constant throughout a stare profile. However, this comes at a cost of a degraded cross-track resolution but due to the multi-static configuration and receiver motion the degradation in cross-track resolution is acceptable. The variable window also reduces the noise in the SMN stare profile.

Further work is required to determine the optimal window profile for a range of scattering geometries. Additionally, the impact of the smoothing effect on MSS retrieval algorithms should be investigated.

ACKNOWLEDGMENTS

The Authors would like to thank Measurement of Earth Reflected Radio-Navigation Signals By Satellite (MERRByS) and Surrey Satellite Technology Ltd (SSTL) for making the data collected by TDS-1 available. This work was supported by the Australian Government through the Research Training Program.

REFERENCES

- [Arroyo et al., 2014] Arroyo, A. A., Camps, A., Aguasca, A., Forte, G. F., Monerris, A., Rüdiger, C., Walker, J. P., Park, H., Pascual, D., and Onrubia, R. (2014). Dual-polarization gnss-r interference pattern technique for soil moisture mapping. *IEEE Journal of Selected Topics in Applied Earth Observations and Remote Sensing*, 7(5):1533–1544.
- [Camps et al., 2016] Camps, A., Park, H., Pablos, M., Foti, G., Gommenginger, C. P., Liu, P.-W., and Judge, J. (2016). Sensitivity of gnss-r spaceborne observations to soil moisture and vegetation. *IEEE Journal of Selected Topics in Applied Earth Observations and Remote Sensing*, 9(10):4730–4742.
- [Clarizia et al., 2009] Clarizia, M., Gommenginger, C., Gleason, S., Srokosz, M., Galdi, C., and Di Bisceglie, M. (2009). Analysis of gnss-r delay-doppler maps from the uk-dmc satellite over the ocean. *Geophysical Research Letters*, 36(2).
- [Clarizia and Ruf, 2016] Clarizia, M. P. and Ruf, C. S. (2016). Wind Speed Retrieval Algorithm for the Cyclone Global Navigation Satellite System (CYGNSS) Mission. *IEEE Transactions on Geoscience and Remote Sensing*, 54(8):4419–4432.
- [Foti et al., 2015] Foti, G., Gommenginger, C., Jales, P., Unwin, M., Shaw, A., Robertson, C., and Roselló, J. (2015). Spaceborne GNSS reflectometry for ocean winds: First results from the UK TechDemoSat-1 mission. *Geophysical Research Letters*, 42(13):5435–5441.
- [Gleason, 2006] Gleason, S. (2006). *Remote sensing of ocean, ice and land surfaces using bistatically reflected GNSS signals from low Earth orbit*. PhD thesis.
- [Gleason et al., 2005] Gleason, S., Hodgart, S., Sun, Y., Gommenginger, C., Mackin, S., Adjrad, M., and Unwin, M. (2005). Detection and processing of bistatically reflected gps signals from

low earth orbit for the purpose of ocean remote sensing. *IEEE Transactions on Geoscience and Remote Sensing*, 43(6):1229–1241.

[Jales, 2012] Jales, P. (2012). *Spaceborne receiver design for scatterometric GNSS reflectometry*. PhD thesis, University of Surrey.

[Martin-Neira, 1993] Martin-Neira, M. (1993). A passive reflectometry and interferometry system (paris): Application to ocean altimetry. *ESA journal*, 17:331–355.

[Rodriguez-Alvarez et al., 2009] Rodriguez-Alvarez, N., Bosch-Lluis, X., Camps, A., Vall-Llossera, M., Valencia, E., Marchan-Hernandez, J. F., and Ramos-Perez, I. (2009). Soil moisture retrieval using gnss-r techniques: experimental results over a bare soil field. *IEEE Transactions on Geoscience and Remote Sensing*, 47(11):3616–3624.

[Ruf et al., 2016] Ruf, C., Clarizia, M., Gleason, S., Jelenak, Z., Murray, J., Morris, M., Musko, S., Posselt, D., Provost, D., Starkenburg, D., and Zavorotny, V. (2016). *CYGNSS Handbook*.

[Ruf et al., 2012] Ruf, C. S., Gleason, S., Jelenak, Z., Katzberg, S., Ridley, A., Rose, R., Scherrer, J., and Zavorotny, V. (2012). The CYGNSS nanosatellite constellation hurricane mission. In *Proc. IEEE Int. Geoscience Remote Sensing Symp.*, pages 214–216, Munich , Germany.

[Schiavulli et al., 2017] Schiavulli, D., Frappart, F., Ramillien, G., Darrozes, J., Nunziata, F., and Migliaccio, M. (2017). Observing Sea/Ice Transition Using Radar Images Generated From TechDemoSat-1 Delay Doppler Maps. *IEEE Geoscience and Remote Sensing Letters*, 14(5):734–738.

[Tye et al., 2016] Tye, J., Jales, P., Unwin, M., and Underwood, C. (2016). The First Application of Stare Processing to Retrieve Mean Square Slope Using the SGR-ReSI GNSS-R Experiment on TDS-1. *IEEE Journal of Selected Topics in Applied Earth Observations and Remote Sensing*, 9(10):4669–4677.

[Zavorotny and Voronovich, 2000] Zavorotny, V. U. and Voronovich, A. G. (2000). Scattering of gps signals from the ocean with wind remote sensing application. *IEEE Transactions on Geoscience and Remote Sensing*, 38(2):951–964.